Accepted Manuscript

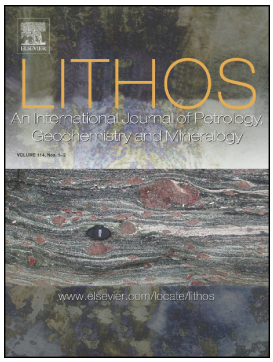

Syn-collisional felsic magmatism and continental crust growth: A case study from the North Qilian Orogenic Belt at the northern margin of the Tibetan Plateau

Shuo Chen, Yaoling Niu, Qiqi Xue

PII: S0024-4937(18)30080-X
DOI: doi:10.1016/j.lithos.2018.03.001
Reference: LITHOS 4589

To appear in:

Received date: 17 November 2017
Accepted date: 5 March 2018

Please cite this article as: Shuo Chen, Yaoling Niu, Qiqi Xue , Syn-collisional felsic magmatism and continental crust growth: A case study from the North Qilian Orogenic Belt at the northern margin of the Tibetan Plateau. The address for the corresponding author was captured as affiliation for all authors. Please check if appropriate. Lithos(2018), doi:10.1016/j.lithos.2018.03.001

Syn-collisional felsic magmatism and continental crust growth: A case study from the North Qilian Orogenic Belt at the northern margin of the Tibetan Plateau

Shuo Chen [1,2,3*], Yaoling Niu [1, 2, 4*], Qiqi Xue [5]

[1] Institute of Oceanology, Chinese Academy of Sciences, Qingdao 266071, China.

[2] Laboratory for Marine Geology, Qingdao National Laboratory for Marine Science and Technology, Qingdao 266061, China

[3] University of Chinese Academy of Sciences, Beijing 100049, China

[4] Department of Earth Sciences, Durham University, Durham DH1 3LE, UK

[5] School of Earth Science and Mineral Resources, China University of Geosciences, Beijing 100083, China.

Corresponding author: chenshuo528@foxmail.com (Shuo Chen); yaoling.niu@durham.ac.uk (Yaoling Niu)

Highlights:

- The two types of MMEs are earlier crystallized cumulate of the same magmas
- The syn-collisional granitoids are material evidence of melting ocean crust
- The syn-collisional magmatism makes a net contribution to continental crust growth.

Abstract

The abundant syn-collisional granitoids produced and preserved at the northern Tibetan Plateau margin provide a prime case for studying the felsic magmatism as well as continental crust growth in response to continental collision. Here we present the results from a systematic study of the syn-collisional granitoids and their mafic magmatic enclaves (MMEs) in the Laohushan (LHS) and Machangshan (MCS) plutons from the North Qilian Orogenic Belt (NQOB). Two types of MMEs from the LHS pluton exhibit identical crystallization age (~430 Ma) and bulk-rock isotopic compositions to their host granitoids, indicating their genetic link. The phase equilibrium constraints and pressure estimates for amphiboles from the LHS pluton together with the whole rock data suggest that the two types of MMEs represent two evolution products of the same hydrous andesitic magmas. In combination with the data on NQOB syn-collisional granitoids elsewhere, we suggest that the syn-collisional granitoids in the NQOB are material evidence of melting of ocean crust and sediment. The remarkable compositional similarity between the LHS granitoids and the model bulk continental crust in terms of major elements, trace elements, and some key element ratios indicates that the syn-collisional magmatism in the NQOB contributes to net continental crust growth, and that the way of continental crust growth in the Phanerozoic through syn-collisional felsic magmatism (production and preservation) is a straightforward process without the need of petrologically and physically complex processes.

Keywords: Mafic magmatic enclaves; Cumulate; Amphibole; Syn-collisional granodiorite; Crust growth

1 Introduction

While the composition of continental crust (CC) has been well established, its origin and way of growth remain enigmatic (Niu et al., 2013). The first-order complementarity between CC and oceanic crust (OC) in terms of incompatible element abundances has been interpreted as the former being extracted from the primitive mantle with the residual depleted mantle as the source of the present-day ocean crust (Hofmann, 1988). Recognizing the similarity between andesite volcanism that occurs at convergent margins and the andesitic bulk CC (BCC) with "arc-like" trace element patterns, Taylor (1967, 1977) proposed that CC growth resulted from subduction zone magmatism, namely the well-known "island-arc model". Subsequent studies, however, have shown that arc crust (AC) is basaltic in bulk composition (Gill, 1981; Rudnick, 1995), and is too mafic for BCC. This marked difference in major element composition between the andesitic BCC and basaltic arc crust has thus been puzzling (Castro et al., 2013; Niu et al., 2013). To resolve this puzzle, several modified versions of island-arc model have been proposed, including (1) delamination of the more mafic deep portions of AC (Kay and Kay, 1993; Rudnick, 1995; Lee et al., 2007); (2) re-lamination of subducted materials in arcs (Hacker et al., 2011); (3) assimilation or mixing between earlier formed felsic rocks (derived from subducted slabs) and mantle-derived mafic magmas (Kelemen, 1995). While these remedies are interesting, problems persist (see review by Niu et al., 2013). For instance, delamination of mafic garnet pyroxenite cumulate ("arclogite"), which needs the formation of garnet to generate favorable density (Lee et al., 2007; Lee and Anderson, 2015), would inevitably result in the arc melts with the "garnet signature" (depleted in heavy rare elements), but the latter is not compatible with the BCC composition (see Niu, 2015). Also, many studies have shown that there is no net crustal growth at neither island arc nor continental arc settings (Niu and O'Hara, 2009) because AC production

and destruction are globally mass balanced (Scholl and von Huene, 2007; Clift et al., 2009). In addition, seafloor spreading/subduction is globally continuous (Condie, 2000), and the "island-arc model" thus cannot account for the episodic CC growth. With all these arc-model difficulties considered and on the basis of their studies on the India-Asia syn-collisional (~55 Ma) andesitic rocks in southern Tibet, Niu and co-authors proposed the hypothesis that "collision zones are primary sites of net continental crustal growth" (Mo et al., 2008; Niu and O'Hara, 2009; Niu et al., 2013).

The continental collision zone hypothesis can be effectively tested because abundant syn-collisional granitoids (and the volcanic counterparts) are well preserved in continental collision zones on the Tibetan Plateau and along the adjacent orogenic belts, which have been shown to record messages on syn-collisional felsic magmatism and CC growth (Mo et al., 2008; Niu et al., 2013; Huang et al., 2014; Chen et al., 2015, 2016; Zhang et al., 2016; Shao et al., 2017). As part of a systematic study of the Early Paleozoic syn-collisional magmatism in the North Qilian Orogenic Belt (NQOB) at the northern Tibetan Plateau margin (Fig. 1a), we present here the results of a comprehensive study of the syn-collisional granitoids and their enclosed mafic magmatic enclaves (MMEs) from the Laohushan (LHS) and Machangshan (MCS) plutons (Fig. 1b). These new data, together with data in the recent literature on syn-collisional granitoids from the NQOB, are used to illustrate (1) the cumulate origin of MMEs, (2) the source of the syn-collisional magmatism, and (3) the mechanisms of CC growth in response to continental collision.

2 Geology and samples

The Qilian orogenic belt (QOB) consists of four nearly NW-SE trending subparallel tectonic units, from north to south, they are: (1) the north Qilian orogenic belt (NQOB), (2) the Qilian

Block (QB), (3) the North Qaidam ultrahigh-pressure metamorphic (NQ-UHPM) belt, and (4) the Qaidam Block (QDB) (Song et al., 2013 and references therein).

The NQOB, extending NW-SE, is separated from the northeastern Alxa Block and the southwestern QB, and from the northwestern Altyn-Tagh Fault (Fig.1a). It represents a typical Early Paleozoic oceanic suture zone, mainly consisting of subduction complexes (Fig. 1a) (Zhang et al., 2007; Song et al., 2007, 2013). Two ophiolite sequences are distributed along the NQOB (Fig. 1a), (i) the southern ophiolite belt, which consists of ultramafic cumulate, peridotite and pillow basalts, represents the oceanic crust formed at an ocean ridge setting (Hou et al., 2006), and (ii) the northern ophiolite belt, which was suggested to generate from a back-arc spreading center (Xia et al., 2003; Xia and Song, 2010).

The QB dominantly consists of Precambrian metamorphic basement, Early Paleozoic intrusive rocks, and Paleozoic to Mesozoic sedimentary sequences (Feng and He, 1996). In the eastern part of the QB, some S-type granitoids (454–445 Ma) (Chen et al., 2008; Huang et al., 2015) and adakitic granitoids (459–440 Ma) (Yang et al., 2015, 2016) have been reported and several different geodynamic processes have been proposed for the origin of these ~450 Ma granitoids, including a syn-collisional setting related to continental collision (Huang et al., 2015), a post-collisional setting resulted from delamination of thickened crust (Chen et al., 2008) or slab break-off (Yang et al., 2015, 2016). Although the exact nature of the QB and the origin of Early Paleozoic intrusive rocks in QB remains debatable, it is notable that our study is focus on the plutons from the NQOB, rather than on the QB. It is thus not comparable in terms of the tectonic background.

The North Qaidam UHPM Belt is dominated by granitic and pelitic gneisses with eclogite lenses. The Qaidam Block has a Precambrian meta-crystalline basement overlain by the

Paleozoic-Mesozoic sedimentary strata (Song et al. 2013).

Different models have been proposed to explain the tectonic evolution in the whole QOB. The most recent comprehensive studies suggest that the NQOB, QB and NQ-UHPM are different products corresponding to one convergence event, during which the subduction was initiated at ~520 Ma, the ocean basin was closed at 440 Ma, exhumation happened around ~420–400 Ma and final orogen collapsed at ~360 Ma (Song et al., 2013). In this model, the NQOB is considered to be an oceanic suture zone, the QB represents an imbricate thrust belt and NQ-UHPM represents a continental-type subduction zone. Accordingly, voluminous granitoids within the island-arc igneous belt across the NQOB have been subdivided into three groups (Song et al., 2013): (1) volcanic arc granitoids (520-460 Ma), (2) syn-collisional granitoids (440-420 Ma) and (3) post-collisional granitoids (<400 Ma).

Five syn-collisional plutons from the NQOB have been recognized; they are, from southeast to northwest, the Qumushan (QMS) pluton (Chen et al., 2016), the Baojishan (BJS) pluton (Chen et al., 2015), the Machangshan (MCS) pluton, the Laohushan (LHS) pluton (Qian et al., 1998), and the Jinfosi (JFS) pluton (Wu et al., 2010; Huang et al., 2017) (Supplementary Table S1 and Fig. 1). MMEs are ubiquitous in these syn-collisional granitoid plutons in the NQOB (Niu et al., 2013; Chen et al., 2015, 2016). These syn-collisional granitoids are mostly not deformed, which is indeed the case for the ~ 55 Ma syn-collisional granitoids in southern Tibet (see Mo et al., 2007, 2008), the ~ 250 Ma syn-collisional granitoids in East Kunlun (Huang et al., 2014, Shao et al., 2017), the ~ 225 Ma syn-collisional granitoids in West Kunlun (Zhang et al., 2016), and the ~ 220 Ma syn-collisional granitoids in West Qinling (Duan et al., 2016).The LHS pluton is an elongate (~2×20 km^2), NW-trending body, which lies east of the NQOB and intruded the Laohushan Ordovician strata (Fig. 1b). It is mainly composed of quartz diorite, granodiorite,

tonalite and minor quartz monzonite (Table S1). Two types of MMEs are recognized and sampled together with their immediate host rocks: (I) samples LHS12-01MME and LHS12-08MME are diorite MMEs (DMME), with a mineral assemblage of plagioclase (~40-50 vol.%), amphibole (~30-48 vol.%), biotite (~2-20 vol.%), quartz (minor-10 vol. %) and accessory minerals (Fig. 2). The DMMEs are of varying size (a few to 10s of centimeters) and shape in sharp contact with the granitoid host (Fig. 2a), resembling MMEs hosted in the BJS and QMS granitoids (Fig. 1b) (Chen et al., 2015, 2016); (II) samples LHS12-05MME, LHS12-06MME and LHS12-10MME are hornblendite MME (HMME), dominated by cumulate amphibole (>90 vol.%) (Fig. S1; Fig. 2) with interstitial plagioclase (~3-5 vol.%), minute clinopyroxene (< 1 vol.%), and accessory minerals such as magnetite, apatite, and zircon. The MCS pluton is about 20 km southeast of the LHS pluton (Fig. 1b). It is dominated by diorite and mainly consists of amphibole, plagioclase, quartz, minor K-feldspar, clinopyroxene and accessory minerals (apatite, zircon, magnetite).

3 Results

Analytical methods for zircon U-Pb dating, minerals composition, bulk-rock major and trace elements, and bulk-rock Sr-Nd-Hf isotopic composition are presented in Supplementary Text S1.

3.1 Zircon U-Pb isotopic results

Zircon U–Pb isotopic data are listed in Supplementary Table S2. Zircons from the LHS host granitoid samples are mostly transparent, euhedral, colorless and show short prismatic forms (~150-300 μm long) with an aspect ratio of 1:1–3:1. They exhibit clear oscillatory zoning of magmatic origin (Fig. S2a). They have varying U (96-331 ppm) and Th (56-140 ppm) with Th/U ratios of 0.38 - 0.69 (Table S2). After rejecting discordant data, thirteen analyses of zircons from

a host granitoid sample yield a weighted mean $^{206}Pb/^{238}U$ age of 433 ±3.1 Ma (Fig. S2a; 1σ, MSWD=0.28, n=13), representing the time of magmatic crystallization.

Zircons from the HMME sample (Type II) are euhedral and show a clear to weakly oscillatory zoning (Fig. S2b). The zircons from the HMMEs exhibit relatively higher U (321 - 2093 ppm) and Th (167 - 1343 ppm), giving similar Th/U ratios of 0.33 - 0.71 to those in zircons of the host granitoids, which indicate the zircons are of magmatic origin (Hoskin and Schaltegger, 2003). Fourteen analyses give a weighted mean $^{206}Pb/^{238}U$ age of 430 ±2.1 Ma (Fig. S2b; 1σ, MSWD=0.83, n=14), the same as the host granitoid within error.

Zircons from the MCS diorite samples are mostly euhedral, prismatic, showing typical oscillatory zoning, and exhibit a smaller size (50 -100 μm) with an aspect ratio of 2:1 - 1:1 (Fig. S2c). They have varying U (117 - 198 ppm) and Th (205 - 284 ppm) with Th/U ratios of 0.56 - 0.81 (Table S2), also suggesting a magmatic origin. After excluding discordant data, zircons from the MCS diorite samples give a weighted mean $^{206}Pb/^{238}U$ ages of 431.4 ± 2.4 Ma (Fig. S2c; 1σ, MSWD = 0.83, n = 13), representing the time of crystallization of the diorite.

The emplacement age of the granitoids and their MMEs from the LHS pluton and diorite from the MCS pluton in the NQOB is identical within error (~430 Ma), which is consistent with the emplacement of BJS and QMS granitoids and their MMEs (Fig. 1b) (Yu et al., 2015; Chen et al., 2015, 2016). It was suggested that the closure time of the Qilian ocean was ~445 Ma, followed by continental collision at ~435-420 Ma (see review by Song et al., 2013). Therefore, these granitoids are the products of a continental collision event.

3.2 Bulk-rock data

Ten representative granitoid host and MME samples (i.e., 5 host-MME pairs) from the LHS

pluton and three diorite samples from the MCS pluton were analyzed for bulk-rock major elements, trace elements and Sr-Nd-Hf isotopic compositions. Their data are presented in Supplementary Table S3.

The LHS host granitoids are calc-alkaline type, ranging from monozonite to granitoid with varying SiO_2 (59.8–63.6 wt.%). They are weakly peraluminous to metaluminous (A/CNK= 0.76 to 1.09), representing typical I-type granite (Fig. 3c) (Chappell and White, 1992). The LHS DMMEs are high-K calc-alkaline and shoshonitic compositions (Fig. 3b), and metaluminous (A/CNK = 0.79 to 0.83) with low SiO_2 (48.8 to 49.4 wt.%) and high MgO (5.8 to 7.5 wt.%). The LHS HMMEs have lower SiO_2 (44.9 to 47.5 wt. %), A/CNK (0.42 to 0.5) and higher MgO (10.8 to 12.3 wt. %) than DMMEs.

Granitoid samples from the LHS pluton are characterized by light REE (LREE) enrichment, relatively flat heavy REE (HREE) patterns (Fig. 4c) with a weak to moderate negative Eu anomaly (Eu/Eu*=0.99-0.73), enriched in large ion lithophile elements (LILE), and depleted in high field strength elements (HFSE; e.g., Nb, Ta and Ti), displaying remarkable similarity to the BCC composition (Fig. 4c, 5a). The REE patterns (Fig. 4c) of the HMME from the LHS pluton are convex with depleted LREE ($(La/Sm)_N < 1$), whereas DMMEs are scoop-shaped, enriched in LREE. They both have higher HREEs (Fig. 4c) than their host rocks, which concurs with their greater modes of REE-enriched mafic minerals. They exhibit depletion in some LILEs (e.g. Th and U) as well as HFSE (Nb, Ta, Zr, Hf and Ti).

The MCS diorites are calc-alkaline and metaluminous (A/CNK = 0.64 to 0.75) with low SiO_2 (51.6 - 54.5 wt.%) and high MgO (7.7 -11.0 wt.%). They have low HREE contents with relatively flat LREE patterns (Fig. 4d) and low degree fractionation of REE ($(La/Yb)_N$=2.9 - 5.0). In the multi-element spider diagram (Fig. 5c), they show LILE enrichment and HFSE

depletion, resembling the LHS DMMEs in terms of REE patterns.

Notably, the two types of MMEs (i.e., DMMEs and HMMEs) from the LHS pluton, diorites from the MCS pluton as well as MMEs from the BJS and QMS plutons are indeed amphibole-rich mafic-diorite or hornblendite with no or minute (<1 vol.%) pyroxene present, despite plotting in the fields ranging from gabbroic diorite, monzogabbro and gabbro (Fig. 3a).

Bulk-rock Sr, Nd, and Hf isotopic compositions of the LHS and MCS plutons in this study as well as those of the BJS and QMS plutons from the literature are summarized in Table S1. The initial $^{87}Sr/^{86}Sr_i$, $\varepsilon_{Nd}(t)$ and $\varepsilon_{Hf}(t)$ are calculated at 430 Ma based on their age data (see Fig. S2 above). The Sr-Nd-Hf isotopic compositions of the LHS DMMEs ($^{87}Sr/^{86}Sr_i$=0.7063 to 0.7094; $\varepsilon_{Nd}(t)$=-2.9 to -2.5; $\varepsilon_{Hf}(t)$=+4.2 to +5.3), HMMEs ($^{87}Sr/^{86}Sr_i$=0.7071 to 0.7075; $\varepsilon_{Nd}(t)$=-4 to -2.5; $\varepsilon_{Hf}(t)$=+5.3 to +6.2) and their host granitoid ($^{87}Sr/^{86}Sr_i$=0.7062 to 0.7101; $\varepsilon_{Nd}(t)$=-3.7 to -2.1; $\varepsilon_{Hf}(t)$=+3.1 to +5.1) are quite similar. Obviously, the initial $^{87}Sr/^{86}Sr_i$, $\varepsilon_{Nd}(t)$ and $\varepsilon_{Hf}(t)$ are indistinguishable with significant overlap within a narrow range for both the host granitoid and the two types of MME samples (Fig. 6d-f; also see Table S3), suggesting that the syn-collisional granitoids in the eastern part of the NQOB formed from coeval and similar parental magmas. In fact, this is also manifested by the correlated variations of $^{87}Rb/^{86}Sr$ vs. $^{87}Sr/^{86}Sr$, $^{147}Sm/^{144}Nd$ vs. $^{143}Nd/^{144}Nd$, and $^{176}Lu/^{177}Hf$ vs. $^{176}Hf/^{177}Hf$ with statistically significant common intercepts or initial ratios (Fig. 6a-c). In addition, the $^{87}Sr/^{86}Sr_i$, $\varepsilon_{Nd}(t)$ and $\varepsilon_{Hf}(t)$ show no correlation with SiO_2 (Fig. 6) and MgO (not shown).

4 Discussion

4.1 Petrogenesis of MMEs of the LHS pluton

The MMEs are ubiquitous in felsic plutons, and their origin has been the subject for over a

century (Pabst, 1928; Dahlquist, 2002; Donaire et al., 2005; Barbarin, 2005; Niu et al., 2013; Chen et al., 2013a; Chen et al., 2015, 2016), during which various models have been proposed, including foreign xenoliths, refractory restite, early crystalized cumulate, and magma mixing between basaltic and felsic magmas.

The crystallization ages and bulk-rock $^{87}Sr/^{86}Sr_i$, $\varepsilon_{Nd}(t)$ and $\varepsilon_{Hf}(t)$ of the two types of MMEs are, within error, indistinguishable from their host granitoids in the LHS pluton (Fig. 6), indicating their genetic link. In fact, the relationships between the DMMEs and their host granitoids in the LHS pluton are texturally and chemically consistent with the observations for the QMS pluton and BJS pluton (Chen et al., 2015, 2016), including (1) the DMMEs have mineral assemblage and mineral compositions resembling their host granitoid (Fig. 2, 7); (2) amphibole grains are compositionally uniform without disequilibrium textures (Fig. 7); (3) their different mineral modal proportions result in the discrepancy of elemental abundances from their host (Fig. 4); (4) significantly, they have indistinguishable $^{87}Sr/^{86}Sr_i$, $\varepsilon_{Nd}(t)$ and $\varepsilon_{Hf}(t)$ compositions with their host granitoids (Fig. 6).

Although the above observations of the DMMEs are consistent with the "autoliths" nature (Pabst, 1928) with the host granitoids, the absence of typical cumulate texture of MMEs has been generally regarded as an evidence against the cumulate origin, but supporting the popular model of magma mixing between mantle-derived mafic and crust-derived felsic magmas (see Barbarin, 2005, Chen et al., 2009). In the model of magma mixing, the fine-grained MMEs represent quench phases of the mafic magma and the same initial isotopic compositions between the host rocks and MMEs are interpreted as resulting from isotopic equilibrium (e.g., Barbarin, 2005). However, this is unlikely because quenching of the mafic melt would have resulted in a markedly contrasting viscosity between the felsic host magma and the solidified MMEs, which

would inevitably restrain mechanical mixing (Farner et al., 2014) and isotopic equilibrium between the two (Chen et al., 2016).

The coeval HMMEs of typical cumulate texture dominated by homogeneous amphibole compositions (Fig. S1, Fig. 7) in this study, are compelling evidence for the cumulate origin of the MMEs. Notably, these petrological observations both agree with experimental studies and geochemical models as illustrated in Fig. 8 (see below). Therefore, the HMMEs and DMMEs in the LHS granitoid host represent the earlier crystallized "mushy" cumulate of the same magmatic systems (see below), which were disturbed by replenishment of subsequent magma and induced melt convection in magma chambers (Chen et al., 2015, 2016).

4.2 Early amphibole crystallization in andesitic melts

Magmatic amphiboles are powerful tools for investigating hydrous magma petrogenesis and evolution (Ribeiro et al., 2016), as their compositional variations are thought to vary as a function of crystallization conditions and host magma composition (Ribeiro et al., 2016; Rooney et al., 2010). The role of fractionation of amphibole from hydrous magma has been recognized in understanding magmatic evolution in volcanic arc systems (Davidson et al., 2007). In this context, it is worth noting that the rarity or absence of amphibole as phenocrysts in most arc volcanic rocks has been puzzling, and has led to the re-revelation of the importance of amphibole in andesitic magma evolution using trace element modeling (Davidson et al., 2007) despite the fact that amphibole is a straightforward liquidus phase during wet andesitic (late stage basaltic) magma evolution (Cawthorn and O'Hara, 1976; Moore and Carmichael, 1998) and that amphibole is a major constituent phase in diorite/granitoid rocks, which are intrusive counterparts of arc volcanic rocks.

In fact, the presence of almost pure amphibole cumulates within HMMEs in our study manifests the petrological significance of amphiboles in calc-alkaline magmatism and also provides significant constraints on the crystallization condition and history of magmas in syn-collisional settings. On the basis of experimental studies, it has been suggested that amphibole should be the first (and sole) liquidus phase at depths in excess of ~7 km until garnet formation at greater depths for water-saturated andesitic magmas (Moore and Carmichael, 1998; Alonso-Perez et al., 2008; Rooney et al., 2010). These experimental studies as well as geochemical studies of amphiboles make it possible to (1) discuss the compositions of the magmas parental to HMMEs as well as DMMEs and their hosts, and to (2) estimate the crystallization conditions.

4.2.1 Magma compositional constraints

As the liquidus phase, amphiboles must record parental magma compositions (Rooney et al., 2010) as manifested by positive correlations between $Mg^{\#}$ ($Mg^{2+}/(Mg^{2+}+Fe^{T})$) of the amphiboles and that of their parental magma during its evolution (Alonso-Perez et al., 2008). The $Mg^{\#}$ of the amphiboles in the LHS HMMEs is 0.65±0.04 (1σ; see Table S4), significantly lower than that of experimental amphiboles (0.75-0.83) (Grove et al., 2003), and that of Baja California amphiboles (0.67-0.80), which were suggested to be in equilibrium with basaltic melts with high $Mg^{\#}$ (Ribeiro et al., 2016), but similar to amphiboles in equilibrium with andesite melt (Alonso-Perez et al., 2008). To evaluate the composition of the magmas parental to the HMMEs and DMMEs, we calculate the $Mg^{\#}$ of the parental magma using equation from Alonso-Perez et al. (2008): $Mg^{\#}_{magma} = 1/\{1+((Fe^{T}/Mg)/Kd^{Fe/Mg})_{amphibole}\}$, where $K_d^{Fe/Mg}=0.38\pm0.04$. Magmas calculated in equilibrium with LHS HMMEs and DMMEs amphiboles have average $Mg^{\#}$ =0.42±0.04 and 0.38±0.04, respectively, which are much lower than that of primitive melts of asthernospheric mantle origin ($Mg^{\#}$ > 0.70) (Grove et al., 2003), suggesting two possible parental melts for the

LHS pluton, (1) they are initial (or primary) andesitic (or basaltic andesite) melt that produced the earlier cumulate MMEs; (2) they are more-evolved melt from basaltic melt, which fractionated some mafic phases (e.g., olivine and/or pyroxene). However, the latter is inconsistent with our observations.

(1) Neither olivine nor pyroxene is observed throughout the syn-collisional plutons in the NQOB, except for minute clinopyroxene (<1% vol.) in the LHS HMMEs and MCS diorites;

(2) It has been well understood that garnet incorporates more of the HREEs ($Kd_{HREE} >> 1$) whereas amphibole incorporates more of MREEs over HREEs. The distribution coefficients of clinopyroxene are insignificant compared to those of amphibole because of Kd_{REE} clinopyroxene << Kd_{REE} amphibole. Thus, as illustrated in Fig. 8, garnet fractionation would increase Dy/Yb with La/Sm increases during differentiation, but amphibole fractionation would decrease Dy/Yb (Davidson et al., 2007). The host granitoids of the LHS and BJS plutons show a decreasing trend of Dy/Yb with differentiation, which concurs with significant amphibole fractionation, rather than garnet or gabbroic assemblage fractionation.

Hence, the most plausible candidate melts parental to the LHS HMMEs are andesitic melt (or basaltic andesite melt), rather than basaltic melts derived from the asthernospheric mantle.

4.2.2 Crystallization conditions

Amphibole is commonly used to calculate crystallization temperatures and pressures (e.g., Hammarstrom and Zen, 1986; Hollister et al., 1987) despite its potential as a geobarometer has been questioned (Erdmann et al., 2014). Recently, Ridolfi et al. (2009) and Ridolfi and Renzulli (2011) presented calibrations that use the compositions of magmatic amphiboles to calculate crystallization temperatures, pressures, fO_2, melt H_2O, and melt compositions. The crystallization

conditions for amphiboles from the LHS DMMEs, HMMEs and their host granitoids are calculated by using these calibrations. As illustrated in Fig. S3, the LHS DMMEs show identical crystallization conditions, including pressure (165±21 MPa), temperature (818±27°C) and H_2O (6.1±0.6wt.%) to their host rocks, which again suggest a cumulate origin for the DMMEs. The HMMEs, however, show higher pressure (328±60 MPa), temperature (908±45°C) and H_2O (7.0±0.5 wt.%) than the DMMEs and their host rocks, indicating that the HMMEs are cumulate of earlier (first and sole) liquidus phase at greater depths (~ 11 km).

These pressure calculations are affirmed by comparing the compositions of amphiboles from the LHS pluton with the experimentally produced amphiboles (Alonso-Perez et al., 2008; Prouteau and Scaillet, 2003; Scaillet and Evans, 1999). To evaluate the potential effects of pressure and temperature on amphibole compositions, we plot the pressure-sensitive indicator of Al^T (superscript T refers to Al content on tetrahedral site) against temperature-sensitive indicator of Na+K (Fig. 9), following a similar approach by Samaniego et al. (2009). The LHS DMMEs and their host (as well as QMS and BJS plutons) with low-Al^T contents overlap the experimental amphibole compositions at 220 MPa and 785–900°C, which matches the pressure calculation using the Al-in-hornblende barometer (see above). In contrast, the HMMEs have higher Al^T, Na+K, and plot close to high pressure amphibole compositions equilibrated at 400 - 800 MPa (Fig. 9) (Prouteau and Scaillet, 2003). While the pressure discrepancy between the calculated using the Al-in-hornblende geobarometer and experimental data may reflect the experimental and model uncertainties, the different crystallization conditions of amphiboles from the HMMEs, DMMEs and their host are obvious.

In summary, the phase equilibrium constraints on hydrous andesitic magmas, the pressure calculations for amphiboles from the LHS pluton as well as the bulk-rock trace elements and Sr-

Nd-Hf isotopic compositions indicate two key stages of crystallization for magmas parental to the LHS pluton, i.e., an early stage under the middle-to-lower crust conditions (400-800 MPa, 900 °C) represented by the fractionation of high-Al^T amphibole, and a late stage under the upper crust conditions (100-200 MPa, 800 °C) characterized by fractionation of plagioclase, low-Al^T amphibole, quartz, and biotite. In fact, the late stage fractionation is also consistent with observations with other syn-collisional plutons in the NQOB (Chen et al., 2015, 2016).

4.3 Constraints on the source

The above discussion on the origin of MMEs as well as the phase equilibrium constraints indicate that the magmas parental to the syn-collisional granitoids and their MMEs in the NQOB are most likely mafic andesitic (or basaltic-andesitic) magmas. Andesitic melts can be generated by wet peridotite melting (O'Hara, 1965), but such melts in equilibrium with mantle peridotite must have elevated MgO content (i.e., high magnesian andesite or HMA) and $Mg^{\#}$ (Tatsumi, 2006). However, the most mafic composition of the LHS host granitoids from the NQOB syn-collisional rock suites has lower MgO (3.27±0.39 wt.%) than HMA (~5- 10 wt.%). In addition, the estimated melts in equilibrium with and parental to the LHS HMME and DMME amphiboles have average $Mg^{\#}$ = 0.42±0.04 and 0.38±0.04, respectively, which are too low compared to HMA ($Mg^{\#}$>0.64) (Tatsumi, 2006). The explanation of magma with low MgO content from very low degree melting of water-saturated mantle peridotite can also be ruled out because such melt produced is volumetrically unimportant (Mo et al., 2008), and cannot account for the voluminous syn-collisional plutons in the NQOB. Therefore, basaltic rock source in abundant is required to melt and generate massive andesitic magmas parental to the plutons in response to the continental collision. Possible candidates are island arc complex through accretion (Kay and Kay, 1993), or thickened lower CC (Xu et al., 2002; Chung et al., 2003), or the remaining

fragments of the oceanic crust (Mo et al., 2008; Niu et al., 2013). As discussed in Chen et al. (2015, 2016), the former two candidates are not applicable in this study, as (1) island arcs are "too shallow and cold", thus unlikely to melt during continental collision because its positive topography (Niu et al., 2003); (2) even if andesitic melt could be generated by deep arc crust cumulate, it would be highly depleted in composition (Tamura, 2009) compared to the observed syn-collisional granitoids (and the MMEs); (3) the syn-collisional granitoids (and the MMEs) in the NQOB have distinctive low K_2O/Na_2O and higher CaO/Al_2O_3 ratios (Fig. 10), which compositionally differ from rocks suggested to be derived from partial melting of the delaminated or thickened lower CC (Li et al., 2016); (4) the whole-rock $\varepsilon_{Hf}(t)$ (4.9±3.8) and $\varepsilon_{Nd}(t)$ (-3.0±1.9) (Fig. S4) of the syn-collisional granitoids (and the MMEs) in the NQOB signifies a significant mantle input (Fig. S4). Hence, the most plausible source of the andesitic magmas parental to the syn-collisional plutons in the NQOB are the remaining fragments of the North Qilian ocean crust, as its melting produces andesitic melts and can also inherit mantle isotopic signatures. As modeled in Fig. S5, binary isotope mixing calculations as done in Chen et al. (2016) can explain the above observations (Fig. S5).

While the subducting ocean crust has long been thought to be thermally insufficient to melt under subduction zones condition (Peacock, 2003) except for some young (and warm) slabs melting where adakite may be produced (Defant and Drummond, 1990), there has been a revived advocacy in recent years that melting of the subducting ocean crust along with sediments is actually needed to explain the geochemical characteristics of some arc lavas (Johnson and Plank, 2000; Elliott, 2003; Gómez-Tuena et al., 2007) and syn-collisional rocks (Mo et al., 2008; Niu et al., 2013; Chen et al., 2015, 2016). According to the "continental collision model" proposed by Niu and co-workers, "the remaining part of North Qilian ocean crust would slowly

subduct/underthrust, and evolve along a path with high T/P because of additional heating by retarded subduction during continental collision, and eventually melt under the amphibolite facies conditions" (see Mo et al., 2008; Niu et a., 2013). We consider that the syn-collisional granitoids in the NQOB in this study are material evidence of melting ocean crust and sediments and this conceptual model explains a multitude of geological observations. Nevertheless, we should note that further effort is required to design specific melting experiments of MORB-derived amphibolites together with terrigenous sediments to quantify trace element budgets and incongruent melting reactions for quantitative modeling (Niu et al., 2013).

4.4 Implications for continental crust growth

The syn-collisional plutons in the NQOB are dominated by mantle isotopic signatures. The particularly significant is the close similarity of the host granitoids to model BCC in terms of both abundances and trace elements patterns (Fig. 4, 5). Thus, the syn-collisional granitoids represent juvenile material and net contribution to CC growth. Because the LHS pluton has the most mafic composition of the syn-collisional granitoids in the NQOB, it is therefore most close to the primary melt and permits us to discuss the CC growth. Fig. 11 compares all the analyzed elements between average host granitoids and two types of MMEs with respect to the BCC. The complementarity between the host granitoids and the MMEs is striking (Fig. 11a, b). An even more striking complementarity between the two is some key incompatible element ratios (Fig. 11c). The primary parental magmas of the LHS granitoid plus the cumulate MMEs are thus mafic andesite in compositions, remarkably resembling the BCC.

This remarkable similarity, however, may be ignored because of the argument that BCC is model dependent, and it stands for a weighted average of idealized endmember compositions over space and time with uncertainties in weighting factors (Lee et al., 2007). Thus, this could be

a coincidence without significance. However, we maintain that the model BCC by Rudnick and Gao (2003) is significant because (1) it is so far the most conscientious work based on numerous efforts in generations using integrated petrological, geochemical, geophysical, and statistical methods; (2) the remarkable compositional similarities between syn-collisional granitoids and the BCC are general observations that have been shown to be the case throughout the Tibetan Plateau, including the mafic andesites of the Linzizong volcanic succession and coeval batholiths in southern Tibet (Mo et al., 2007, 2008), and syn-collisional granitoids in East and West Kunlun orogens (Huang et al., 2014; Shao et al., 2017; Zhang et al., 2016) and West Qingling orogen (Duan et al., 2016;). Therefore, Fig.s 5 and 11 illustrate five key points: (1) while the CC is complex and heterogeneous in lithologies, the model BCC composition by Rudnick and Gao (2003) is at present the best representation of the CC (Mo et al., 2008); (2) the host granitoids and the MMEs are different end products of the same magma system with the MMEs being of cumulate origin; (3) the primary melts parental to the syn-collisional LHS granitoids and the MMEs compositionally highly resembles the BCC; (4) The syn-collisional felsic magmatism, such as represented by the syn-collisional plutons in the NQOB, contributes to net CC growth as they are juvenile crustal materials generated from the mantle source recently through a transition of ocean crust formation (Mo et al., 2008); (5) the way of CC growth in the Phanerozoic through syn-collisional felsic magmatism is straightforward and does not require complex processes compared to other models, such as the popular “island-arc” model, which requires physically complex and unlikely process to remove the more mafic component from the AC (e.g., Kay and Kay, 1993; Rudnick, 1995; Lee et al., 2007; Lee and Andersen, 2015) so as to convert bulk AC to the BCC. Therefore, these syn-collisional granitoids and MMEs in the NQOB offer new evidence in support of the hypothesis that continental collision zones are the primary sites where

the net CC is accreted and preserved.

5 Concluding Remarks

We identify two types of MMEs in the LHS pluton from the NQOB, which are coeval and have indistinguishable bulk-rock initial Sr, Nd, and Hf isotopic compositions with their granitoid host, suggesting that the MMEs concur with being earlier crystallized cumulate of the same magmatic systems. The phase equilibrium constraints and pressure estimates for amphiboles in the LHS pluton together with the whole rock data further indicate that the two lithologies represent two evolution products of the same hydrous andesitic magmas. The syn-collisional granitoids in the NQOB presented here are material evidence of melting ocean crust and sediments. The remarkable compositional similarity between the LHS granitoid pluton (MMEs and the host granitoid) and the model BCC indicate that the syn-collisional magmatism such as in the NQOB makes a net contribution to the mass of CC, and that the way of CC growth in the Phanerozoic through syn-collisional felsic magmatism (production and preservation) is straightforward and does not require complex and physically unlikely processes.

Acknowledgments

We are grateful to Li Su, Minwu Liu, and Jinlong Ma for their technical support. Jiyong Li, Pu Sun, Wenli Sun, Huixiang Cui, Yu Zhang, and Yuxing Ma are thanked for their help with field investigation and sample preparation. We also thank editor Xian-Hua Li for handling this manuscript and two anonymous reviewers for constructive comments and suggestions. This work was supported by the NSFC-Shandong Joint Fund for Marine Science Research Centers (U1606401) and NSFC grant (41630968, 41130314, 41776067). SC acknowledges the fellowship from the UCAS Joint Ph.D. Training Program (UCAS[2015]37).

References

Alonso-Perez, R., Müntener, O., Ulmer, P., 2009. Igneous garnet and amphibole fractionation in the roots of island arcs: experimental constraints on andesitic liquids. Contributions to Mineralogy and Petrology 157, 541-558.

Barbarin, B., 2005. Mafic magmatic enclaves and mafic rocks associated with some granitoids of the central Sierra Nevada batholith, California: nature, origin, and relations with the hosts. Lithos 80, 155-177.

Cawthorn, R.G., O'hara, M.J., 1976. Amphibole fractionation in calc-alkaline magma genesis. American Journal of Science 276, 309-329.

Castro, A., Vogt, K., Gerya, T., 2013. Generation of new continental crust by sublithospheric silicic-magma relamination in arcs: A test of Taylor's andesite model. Gondwana Research 23, 1554-1566.

Chappell, B. White, A., 1992. I-and S-type granites in the Lachlan Fold Belt. Geological Society of America Special Papers 272, 1-26.

Chen, B., Chen, Z. C., Jahn, B. M., 2009. Origin of mafic enclaves from the Taihang Mesozoic orogen, north China craton. Lithos 110, 343-358.

Chen, B., Jahn, B. M., Suzuki, K., 2013a. Petrological and Nd-Sr-Os isotopic constraints on the origin of high-Mg adakitic the North China Craton: Tectonic implications. Geology 41, 91-94.

Chen, J.L., Xu, X.Y., Zeng, G.X., Xiao, L.,Wang, H.L., Wang, Z.Q., Xiao, S.W., 2008. Geochemical characters and LA-ICPMS zircon U–Pb dating constraints on the petrogenesis and tectonic setting of the Shichuan intrusion, east segment of the Central Qilian, NW China. Acta Petrologica Sinica 24, 841–854 (in Chinese with English abstract).Chen, S., Niu, Y., Li, J., Sun, W., Zhang, Y., Hu, Y., Shao, F., 2016. Syn-collisional adakitic granodiorites formed by fractional crystallization: Insights from their enclosed mafic magmatic enclaves (MMEs) in the Qumushan pluton, North Qilian Orogen at the northern margin of the Tibetan Plateau. Lithos 248-251, 455-468.

Chen, S., Niu, Y., Sun, W., Zhang, Y., Li, J., Guo, P., Sun, P., 2015. On the origin of mafic magmatic enclaves (MMEs) in syn-collisional granitoids: evidence from the Baojishan pluton in the North Qilian Orogen, China. Mineralogy and Petrology 109, 577-596.

Chung, S.-L., Liu, D., Ji, J., Chu, M.-F., Lee, H.-Y., Wen, D.-J., Lo, C.-H., Lee, T.-Y., Qian, Q., Zhang, Q., 2003. Adakites from continental collision zones: Melting of thickened lower crust beneath southern Tibet. Geology 31, 1021.

Clift, P. D., Schouten, H., Vannucchi, P., 2009. Arc-continent collisions, sediment recycling and the maintenance of the continental crust. Geological Society, London, Special Publications 318, 75-103.

Condie, K. C., 2000. Episodic continental growth models: afterthoughts and extensions. Tectonophysics 322, 153-162.

Dahlquist, J., 2002. Mafic microgranular enclaves: early segregation from metaluminous magma (Sierra de Chepes), Pampean Ranges, NW Argentina. Journal of South American Earth Sciences 15, 643-655.

Davidson, J., Turner, S., Handley, H., Macpherson, C., Dosseto, A., 2007. Amphibole "sponge" in arc crust? Geology 35, 787.

Defant, M. J. Drummond, M. S., 1990. Derivation of some modern arc magmas by melting of young subducted lithosphere. Nature 347, 662-665.

Donaire, T., Pascual, E., Pin, C., Duthou, J.-L., 2005. Microgranular enclaves as evidence of rapid cooling in granitoid rocks: the case of the Los Pedroches granodiorite, Iberian Massif, Spain. Contributions to Mineralogy and Petrology 149, 247-265.

Duan, M., Y. Niu, J. Kong, P. Sun, Y. Hu, Y. Zhang, S. Chen, and J. Li, 2016. Zircon U–Pb geochronology, Sr–Nd–Hf isotopic composition and geological significance of the Late Triassic Baijiazhuang and Lvjing granitic plutons in West Qinling Orogen. Lithos 260, 443-456.

Elliott T., 2003. Tracers of the Slab. Inside the Subduction Factory. American Geophysical Union, Geophysical Monograph 138, 23-45.

Erdmann, S., Martel, C., Pichavant, M., Kushnir, A., 2014. Amphibole as an archivist of magmatic crystallization conditions: problems, potential, and implications for inferring magma storage prior to the paroxysmal 2010 eruption of Mount Merapi, Indonesia. Contributions to Mineralogy and Petrology 167.

Farner, M. J., C.-T. A. Lee, and K. D. Putirka, 2014. Mafic–felsic magma mixing limited by reactive processes: a case study of biotite-rich rinds on mafic enclaves. Earth and Planetary Science Letters 393, 49-59.

Feng, Y.M., He, S.P., 1996. Geotectonics and Orogeny of the Qilian Mountains. Geological Publish House, Beijing.

Gómez-Tuena, A., Langmuir, C. H., Goldstein, S. L., Straub, S. M., Ortega-Gutiérrez, F., 2007. Geochemical Evidence for Slab Melting in the Trans-Mexican Volcanic Belt. Journal of Petrology 48, 537-562.

Gill, J., 1981. Orogenic Andesites and Plate. Tectonics, Springer-Verlag, New York.

Grove, T. L., Elkins-Tanton, L. T., Parman, S. W., Chatterjee, N., Mntener, O., Gaetani, G. A., 2003. Fractional crystallization and mantle-melting controls on calc-alkaline differentiation trends. Contributions to Mineralogy and Petrology 145, 515-533.

Hacker, B. R., Kelemen, P. B., Behn, M. D., 2011. Differentiation of the continental crust by relamination. Earth and Planetary Science Letters 307, 501-516.

Hammarstrom, J. M. Zen, E., 1986. Aluminum in hornblende; an empirical igneous geobarometer. American Mineralogist 71, 1297-1313.

Hofmann, A. W., 1988. Chemical differentiation of the Earth: the relationship between mantle, continental crust, and oceanic crust. Earth and Planetary Science Letters 90, 297-314.

Hollister, L. S., Grissom, G. C., Peters, E. K., Stowell, H. H., Sisson, V. B., 1987. Confirmation of the empirical correlation of Al in hornblende with pressure of solidification of calc-alkaline plutons. American Mineralogist 72, 231–239.

Hou, Q., Chen, Y., Zhao, Z., Zhang, H., Zhang, B., 2006. Indian Ocean-MORB-type isotopic signature of Yushigou ophiolite in North Qilian Mountains and its implications. Science in China Series D-Earth Science 49, 561-572.

Huang, H., Niu, Y., Mo, X., 2017. Garnet effect on Nd-Hf isotope decoupling: Evidence from the Jinfosi batholith, Northern Tibetan Plateau. Lithos 274-275, 31-38.

Huang, H., Niu, Y., Nowell, G., Zhao, Z., Yu, X., Zhu, D.-C., Mo, X., Ding, S., 2014. Geochemical constraints on the petrogenesis of granitoids in the East Kunlun Orogenic belt, northern Tibetan Plateau: Implications for continental crust growth through syn-collisional felsic magmatism. Chemical Geology 370, 1-18.

Huang, H., Niu, Y., Nowell, G., Zhao, Z., Yu, X., Mo, X., 2015. The nature and history of the Qilian Block in the context of the development of the Greater Tibetan Plateau. Gondwana Research 28, 209-224.

Johnson, M. C. Plank, T., 2000. Dehydration and melting experiments constrain the fate of subducted sediments. Geochemistry, Geophysics, Geosystems 1, paper number 1999GC000014.

Kay, R. W. Kay, S. M., 1993. Delamination and delamination magmatism. Tectonophysics 219, 177-189.

Kelemen, P. B., 1995. Genesis of high Mg# andesites and the continental crust. Contributions to Mineralogy and Petrology 120, 1-19.Lee, C.-T. A. Anderson, D. L., 2015. Continental crust formation at arcs, the arclogite "delamination" cycle, and one origin for fertile melting anomalies in the mantle. Science Bulletin 60, 1141-1156.

Lee, C.-T. A., Morton, D. M., Kistler, R. W., Baird, A. K., 2007. Petrology and tectonics of Phanerozoic continent formation: From island arcs to accretion and continental arc magmatism. Earth and Planetary Science Letters 263, 370-387.

Li, S.-M., Zhu, D.-C., Wang, Q., Zhao, Z., Zhang, L.-L., Liu, S.-A., Chang, Q.-S., Lu, Y.-H., Dai, J.-G., Zheng, Y.-C., 2016. Slab-derived adakites and subslab asthenosphere-derived OIB-type rocks at 156±2Ma from the north of Gerze, central Tibet: Records of the Bangong–Nujiang oceanic ridge subduction during the Late Jurassic. Lithos 262, 456-469.

Macpherson, C. G., Dreher, S. T., Thirlwall, M. F., 2006. Adakites without slab melting: High pressure differentiation of island arc magma, Mindanao, the Philippines. Earth and Planetary Science Letters 243, 581-593.

Mo, X.X., Hou, Z.Q., Niu, Y.L., Dong, G.C., Qu, X.M., Zhao, Z.D., Yang, Z.M., 2007. Mantle contributions to crustal thickening in south Tibet in response to the India-Asia collision. Lithos 96, 225-242.

Mo, X., Niu, Y., Dong, G., Zhao, Z., Hou, Z., Zhou, S., Ke, S., 2008. Contribution of syncollisional felsic magmatism to continental crust growth: A case study of the Paleogene Linzizong volcanic Succession in southern Tibet. Chemical Geology 250, 49-67.Moore, G. Carmichael, I. S. E., 1998. The hydrous phase equilibria (to 3 kbar) of an andesite and basaltic andesite from western Mexico: constraints on water content and conditions of phenocryst growth. Contributions to Mineralogy and Petrology 130, 304-319.

Niu, Y.L., 2015. How and where does continental xrust form? Science Bulletin 60, 1139-1140.

Niu, Y.L., and M. J. O'Hara, 2003. Origin of ocean island basalts: A new perspective from petrology, geochemistry,

and mineral physics considerations, Journal of Geophysical Research: Solid Earth 108.B4

Niu, Y. O'Hara, M. J., 2009. MORB mantle hosts the missing Eu (Sr, Nb, Ta and Ti) in the continental crust: New perspectives on crustal growth, crust–mantle differentiation and chemical structure of oceanic upper mantle. Lithos 112, 1-17.

Niu, Y., Zhao, Z., Zhu, D.-C., Mo, X., 2013. Continental collision zones are primary sites for net continental crust growth — A testable hypothesis. Earth-Science Reviews 127, 96-110.

O'Hara, M. J., 1965. Primary magmas and the origin of basalts. Scottish Journal of Geology 1, 19-40.

Pabst, A.,, 1928. Observations on inclusions in the granitic rocks of the Sierra Nevada. University of California. Publications in Geological Science 17, 325–386.

Peacock, S.M., 2003. Thermal structure and metamorphic evolution of subducting slabs . Geophysical Monograph 238, 7–22.

Prouteau, G. Scaillet, B., 2003. Experimental Constraints on the Origin of the 1991 Pinatubo Dacite. Journal of Petrology 44, 2203-2241.

Qian, Q., Wang, Y., Li, H., Jia, X., Zhang, Q., 1998. Geochemical Characteristics and Genesis of Diorites from Laohushan, Gansu Province. Acta Petrologica Sinica 14, 520–528 (in Chinese with English abstract).

Ribeiro, J. M., Maury, R. C., Grégoire, M., 2016. Are Adakites Slab Melts or High-pressure Fractionated Mantle Melts? Journal of Petrology 57, 839-862.

Ridolfi, F. Renzulli, A., 2011. Calcic amphiboles in calc-alkaline and alkaline magmas: thermobarometric and chemometric empirical equations valid up to 1,130°C and 2.2 GPa. Contributions to Mineralogy and Petrology 163, 877-895.

Ridolfi, F., Renzulli, A., Puerini, M., 2009. Stability and chemical equilibrium of amphibole in calc-alkaline magmas: an overview, new thermobarometric formulations and application to subduction-related volcanoes. Contributions to Mineralogy and Petrology 160, 45-66.

Rooney, T. O., Franceschi, P., Hall, C. M., 2010. Water-saturated magmas in the Panama Canal region: a precursor to adakite-like magma generation? Contributions to Mineralogy and Petrology 161, 373-388.

Rudnick, R. Gao, S., 2003. Composition of the continental crust. Treatise on geochemistry 3, 659.

Rudnick, R. L., 1995. Making continental crust. Nature 378, 571.

Samaniego, P., C. Robin, G. Chazot, E. Bourdon, and J. Cotten, 2009), Evolving metasomatic agent in the Northern Andean subduction zone, deduced from magma composition of the long-lived Pichincha volcanic complex (Ecuador). Contributions to Mineralogy and Petrology 160(2), 239-260.

Scaillet, B. Evans, B. W., 1999. The 15 June 1991 Eruption of Mount Pinatubo. I. Phase Equilibria and Pre-eruption P–T–fO_2–fH_2O Conditions of the Dacite Magma. Journal of Petrology 40, 381-411(331).

Scholl, D. W. von Huene, R., 2007. Crustal recycling at modern subduction zones applied to the past—Issues of growth and preservation of continental basement crust, mantle geochemistry, and supercontinent reconstruction. Geological Society of America Memoirs 200, 9-32.

Shao, F.L., Niu, Y.L., Liu, Y., Chen, S., Kong, J.J., Duan, M., 2017. Petrogenesis of Triassic granitoids in the East Kunlun Orogenic Belt, northern Tibetain Plateau and their tectonic implications. Lithos 282-283, 33-44.

Shaw, D. M., 1970. Trace element fractionation during anatexis. Geochimica et Cosmochimica Acta 34(2), 237-243.

Song, S., Niu, Y., Su, L., Xia, X., 2013. Tectonics of the North Qilian orogen, NW China. Gondwana Research 23, 1378-1401.

Song, S. G., Zhang, L. F., Niu, Y., Wei, C. J., Liou, J. G., Shu, G. M., 2007. Eclogite and carpholite-bearing metasedimentary rocks in the North Qilian suture zone, NW China: implications for Early Palaeozoic cold oceanic subduction and water transport into mantle. Journal of Metamorphic Geology 25, 547-563.

Tamura, Y., 2009. Silicic Magmas in the Izu–Bonin Oceanic Arc and Implications for Crustal Evolution. Journal of Petrology 50, 685-723.

Tatsumi, Y., 2006. High-mg andesites in the setouchi volcanic belt, southwestern japan: analogy to Archean Magmatism and Continental Crust Formation? Annual Review of Earth Planetary Sciences 34, 467-499.

Taylor, S. R., 1967. The origin and growth of continents. Tectonophysics 4, 17-34.

Taylor, S. R., 1977. Island arc models and the composition of the continental crust. Island arcs, deep sea trenches and back-arc basins, 325-335.

Tseng, C.-Y., Yang, H.-J., Yang, H.-Y., Liu, D., Wu, C., Cheng, C.-K., Chen, C.-H., Ker, C.-M., 2009. Continuity of the North Qilian and North Qinling orogenic belts, Central Orogenic System of China: Evidence from newly discovered Paleozoic adakitic rocks. Gondwana Research 16, 285-293.

Wang, C. Y., Zhang, Q., Qian, Q., Zhou, M. F., 2005a. Geochemistry of the Early Paleozoic Baiyin Volcanic Rocks (NW China): Implications for the Tectonic Evolution of the North Qilian Orogenic Belt. The Journal of Geology 113, 83-94.

Wang, J., Wu, C., Cai, Z., Guo, Y., Wu, J., Liu, X., 2006. Early Paleozoic high-Mg adakite from Yindongliang in the eastern section of the North Qilian: Implications for geodynamics and Cu-Au mineralization. Acta Petrologica Sinica 22, 2655-2664 (in Chinese with English abstract).

Wu, C. L., Xu, X. Y., Gao, Q. M., Li, X. M., Lei, M., Gao, Y. H., Frost, R. B., Wooden, J. L., 2010. Early Paleozoic granitoid magmatism and tectonic evolution in North Qilian, NW China. Acta Petrologica Sinica 26, 1027-1044 (in Chinese with English abstract).

Xia, L. Q., Xia, Z. C., Xu, X. Y., 2003. Magmagenesis in the Ordovician backarc basins of the Northern Oilian Mountains,China. Geological Society of America Bulletin 115, 1510-1522.

Xia, X., Song, S., Niu, Y., 2012. Tholeiite–Boninite terrane in the North Qilian suture zone: Implications for subduction initiation and back-arc basin development. Chemical Geology 328, 259-277.

Xia, X. H. Song, S. G., 2010. Forming age and tectono-petrogenises of the Jiugequan ophiolite in the North Qilian Mountain, NW China. Science Bulletin 55, 1899-1907.

Xu, J.-F., Shinjo, R., Defant, M. J., Wang, Q., Rapp, R. P., 2002. Origin of Mesozoic adakitic intrusive rocks in the Ningzhen area of east China: Partial melting of delaminated lower continental crust? Geology 30, 1111.

Yang, H., Zhang, H.F., Luo, B.J., Zhang, J., Xiong, Z.L., Guo, L., Pan, F.B., 2015. Early Paleozoic intrusive rocks from the eastern Qilian orogen, NE Tibetan Plateau: petrogenesis and tectonic significance. Lithos 224, 13–31.

Yang, H., Zhang, H., Luo, B., Gao, Z., Guo, L., Xu, W., 2016. Generation of peraluminous granitic magma in a post-collisional setting: A case study from the eastern Qilian orogen, NE Tibetan Plateau. Gondwana Research 36, 28-45.

Yu, S., Zhang, J., Qin, H., Sun, D., Zhao, X., Cong, F., Li, Y., 2015. Petrogenesis of the early Paleozoic low-Mg and

high-Mg adakitic rocks in the North Qilian orogenic belt, NW China: Implications for transition from crustal thickening to extension thinning. Journal of Asian Earth Sciences 107, 122-139.

Zhang, J. X., Meng, F. C., Wan, Y. S., 2007. A cold Early Palaeozoic subduction zone in the North Qilian Mountains, NW China: petrological and U-Pb geochronological constraints. Journal of Metamorphic Geology 25, 285-304.

Zhang, Y., Niu, Y., Hu, Y., Liu, J., Ye, L., Kong, J., Duan, M., 2016. The syncollisional granitoid magmatism and continental crust growth in the West Kunlun Orogen, China – Evidence from geochronology and geochemistry of the Arkarz pluton. Lithos 245, 191-204.

Figure captions

Fig. 1. (a) Simplified geological map of the North Qilian Orogenic Belt (NQOB) showing the main tectonic units (modified after Chen et al., 2016). (b) Simplified map of the Qumushan (QMS), Baojishan (BJS), Machangshan (MCS) and Laohushan (LHS) plutons in the eastern section of the NQOB. U-Pb ages for the syn-collisional granodiorite and enclosed MMEs are from Chen et al. (2015, 2016), Yu et al. (2015) and this study as indicated.

Fig. 2. Field (a-b) and thin-section (c-f) photographs of the granitoid and the MMEs in the LHS pluton. (a) and (b) showing the sharp contact of two types (D and H) of MMEs with their host granitoid; (c) (e) and (f) showing the mineral assemblage of HMMEs; (d) showing the mineral assemblage of the host granitoid. Amp = amphibole; Bi = biotite; Pl= plagioclase; Qz = quartz.

Fig. 3. Classification diagrams of the syn-collisional granitoids (circles) and their hosted MMEs (squares) from the NQOB. (a) Total alkalis vs. SiO_2 (Le Maitre et al., 1989), (b) K_2O vs. SiO_2, and (c) A/NK vs. A/CNK. The LHS samples are in yellow. The green squares are MMEs of the MCS pluton. The literature data on the syn-collisional granitoids from the NQOB are plotted for

comparison: grey symbols for the BJS granitoids (Chen et al., 2015), and purple symbols for the QMS granitoids (Tseng et al., 2009; Chen et al., 2016).

Fig. 4. Chondrite normalized REE patterns for syn-collisional granitoids and the MMEs from the NQOB. (a), (b) (c) and (d) showing data on samples from BJS, QMS, MCS and LHS plutons, respectively. BCC refers to model bulk continental crust composition (Rudnick and Gao, 2003).

Fig. 5. Average ocean crust-normalized (OC) (Niu and O'Hara, 2003) trace element patterns for syn-collisional granitoids and the MMEs from the NQOB. Symbols are the same as in Fig. 4.

Fig. 6. (a-c) Plots of isotopic ratios vs. parent–daughter ratios for granitoids and the MMEs from the LHS and MCS pluton, showing they have statistically significant common intercepts or initial ratios. (d-e) Plots of Sr-Nd-Hf isotopes vs. SiO_2, showing similar or significantly overlapping isotopes between MMEs and their granitoid hosts, and they show no correlated variations with SiO_2.

Fig. 7. Compositional traverses for selected amphibole crystals with thin-section images from the LHS granitoids, and the hosted DMMEs and HMMEs (a, b, c). Spot numbers along the traverses correspond to the compositional variations ($Mg^{\#}$, Ca, and Al^{T}) plotted on the right (d, e, f). See Table S4 for compositional data. See text for detailed discussion.

Fig. 8. Diagrams of La/Yb vs. La/Sm (a) and Dy/Yb vs. La/Sm (b) showing the effects of fractional crystallization during magma evolution of the syn-collisional granitoids in the NQOB. The fractional crystallization modeling uses the Rayleigh fractionation equation $C_{liquid} = C_{initial} \times F^{(D-1)}$ (Shaw, 1970), where F is the fraction of liquid remains and D is the bulk distribution coefficients. The initial concentrations and D values for elements of interest and relevant

minerals are given in Supplementary Table S5. Model fractionation curves are assemblages of LHS DMME (Model A), LHS HMME (Model B), a nominal gabbro comprising 20% olivine, 35% clinopyroxene, and 35% plagioclase (Model C) (Davidson et al., 2007) and experimental assemblages of Rapp and Watson (1995) (R&W, Model D and E). Vectors for Surigao (Philippines) are shown as examples of suites that have fractionated garnet (Macpherson et al., 2006). Abbreviations: Cpx-clinopyroxene; Amp—amphibole; Grt—garnet; Pl—plagioclase.

Fig. 9. Diagram Al^T vs. Na + K of amphiboles used to estimate crystallization pressures for the syn-collisional granitoids and the MMEs from the NQOB. The amphibole compositions, determined using PROBE AMPH (Leake, 1978), are compared with compositions of experimental amphiboles (Prouteau et al., 1999; Scaillet and Evans, 1999; Alonso-Perez et al., 2008) to infer magma storage depths.

Fig. 10. K_2O/Na_2O vs. CaO/Al_2O_3 diagram showing the difference between slab-derived adakites and lower crust-derived adakites. Data sources: typical adakites resulting from partial melting of subducted ocean crust in modern arcs (from the GeoRoc database: http://georoc.mpch-mainz.gwdg.de/georoc/) and adakitic rocks from southern Tibet (Chung et al., 2003; Wang et al., 2005) and Dabie Orogen (He et al., 2013; Wang et al., 2007).

Fig. 11. Average major elements (a), trace elements (b) and selected key incompatible trace element ratios (c) of the LHS granitoids and the MMEs divided by bulk continental crust composition (Rudnick and Gao, 2003).

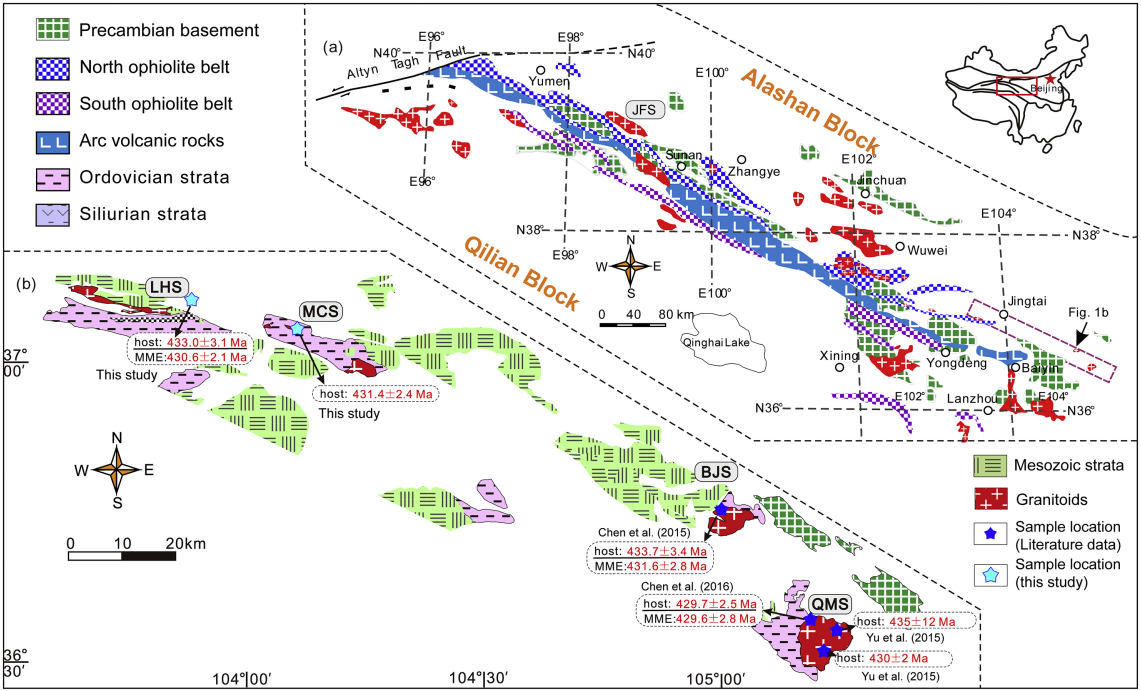
Precambian basement
North ophiolite belt
South ophiolite belt
Arc volcanic rocks
Ordovician strata
Siliurian strata
(a)
Altyn Tagh Fault
E96°
E98°
E100°
E102°
E104°
N40°
N38°
N36°
Yumen
Sunan
Zhangye
Liuchuan
Wuwei
Jingtai
Fig. 1b
Xining
Yongdeng
Lanzhou
Baiyin
Qinghai Lake
JFS
Alashan Block
Qilian Block
Beijing
0 40 80 km
(b)
LHS
MCS
BJS
QMS
host: 433.0±3.1 Ma
MME:430.6±2.1 Ma
This study
host: 431.4±2.4 Ma
This study
Chen et al. (2015)
host: 433.7±3.4 Ma
MME:431.6±2.8 Ma
Chen et al. (2016)
host: 429.7±2.5 Ma
MME:429.6±2.8 Ma
host: 435±12 Ma
Yu et al. (2015)
host: 430±2 Ma
Yu et al. (2015)
0 10 20km
37° 00′
36° 30′
104°00′
104°30′
105°00′
Mesozoic strata
Granitoids
Sample location (Literature data)
Sample location (this study)

Figure 1

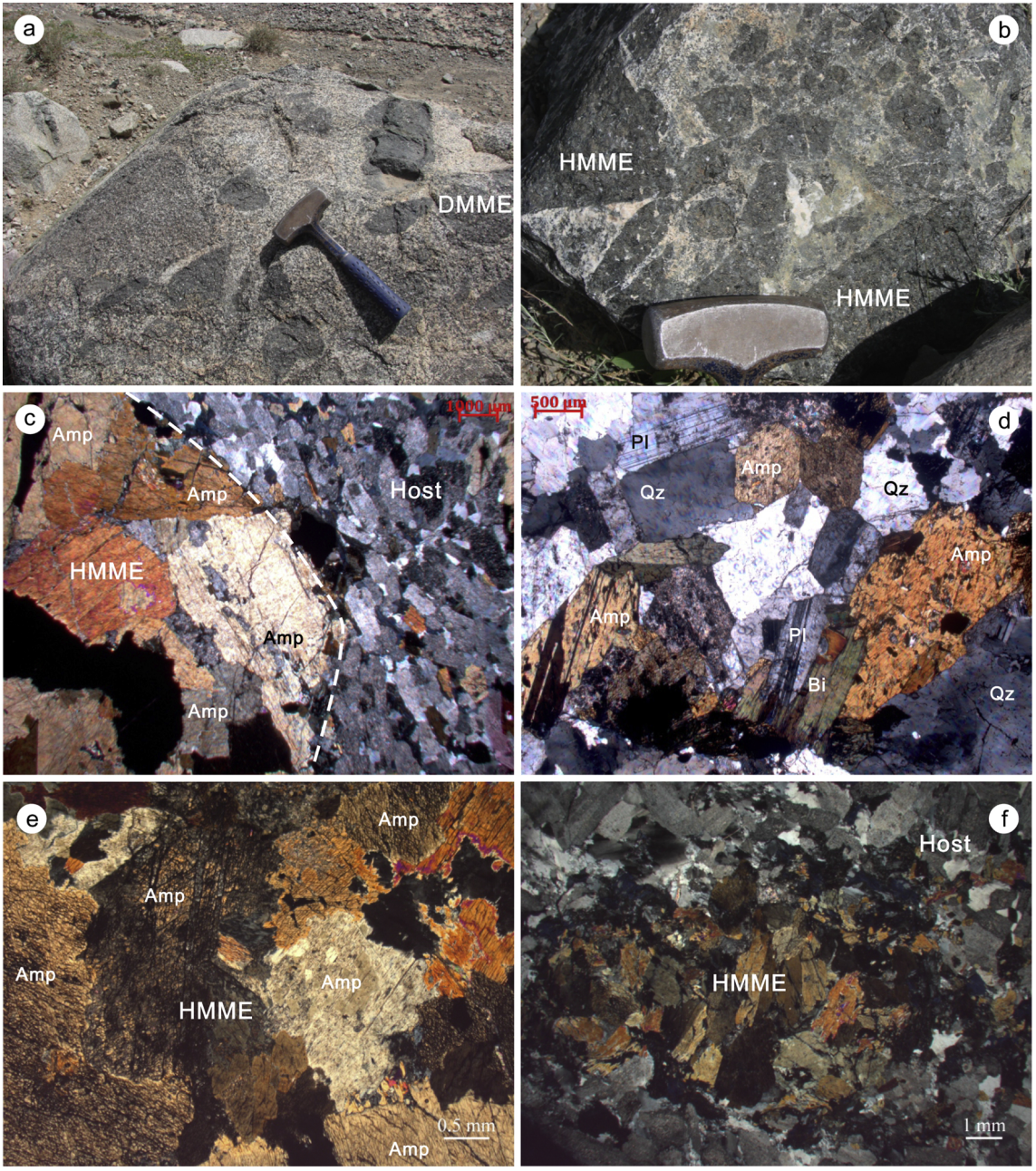
a
DMME
b
HMME
HMME
c
1000 μm
Amp
Amp
Host
HMME
Amp
Amp
500 μm
d
Pl
Amp
Qz
Qz
Amp
Amp
Pl
Bi
Qz
e
Amp
Amp
Amp
Amp
HMME
0.5 mm
Amp
f
Host
HMME
1 mm

Figure 2

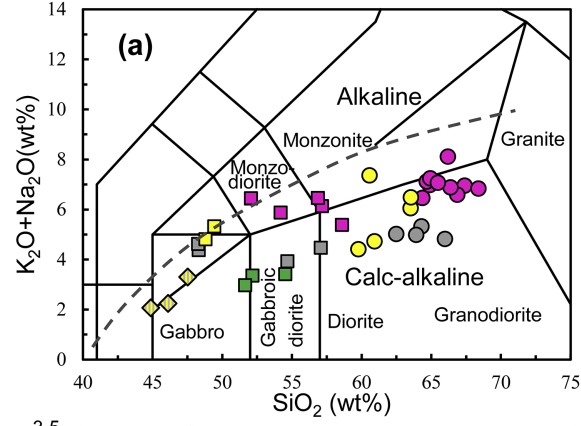
(a)
Alkaline
Monzonite
Granite
Monzo-diorite
Calc-alkaline
Gabbro
Gabbroic diorite
Diorite
Granodiorite
K_2O+Na_2O(wt%)
SiO_2 (wt%)

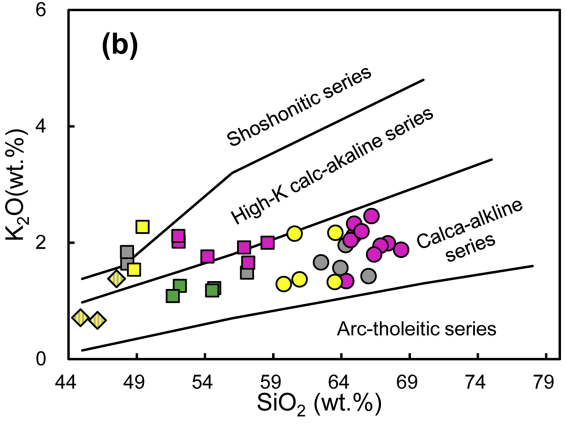
(b)
Shoshonitic series
High-K calc-akaline series
Calca-alkline series
Arc-tholeitic series
K_2O(wt.%)
SiO_2 (wt.%)

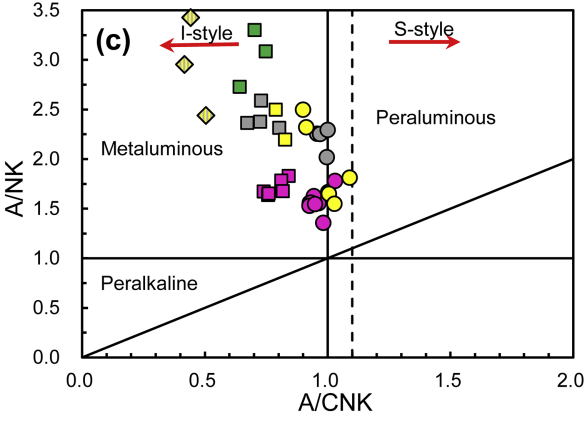
(c)
I-style
S-style
Peraluminous
Metaluminous
Peralkaline
A/NK
A/CNK

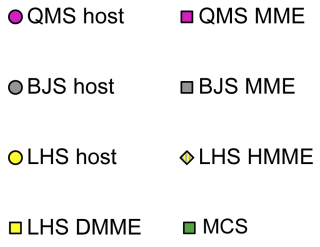
QMS host
QMS MME
BJS host
BJS MME
LHS host
LHS HMME
LHS DMME
MCS

Figure 3

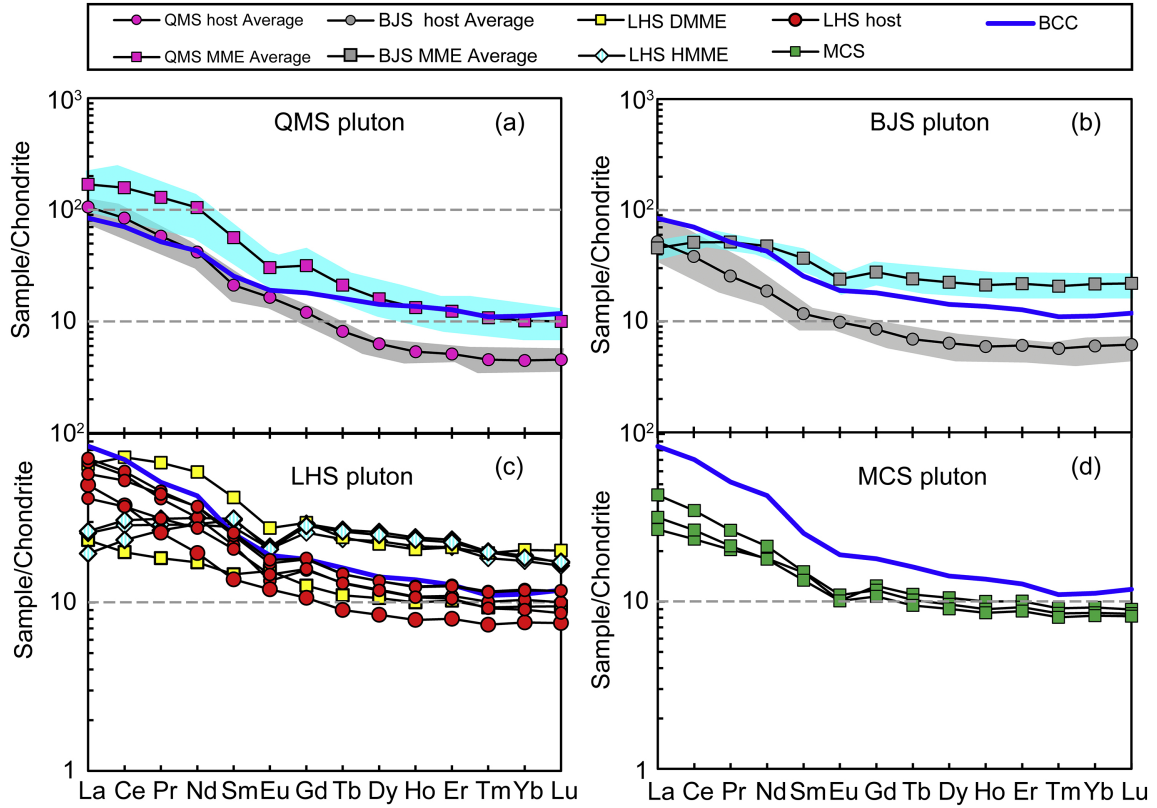
QMS host Average
BJS host Average
LHS DMME
LHS host
BCC
QMS MME Average
BJS MME Average
LHS HMME
MCS
QMS pluton
(a)
BJS pluton
(b)
LHS pluton
(c)
MCS pluton
(d)
Sample/Chondrite
La Ce Pr Nd Sm Eu Gd Tb Dy Ho Er Tm Yb Lu

Figure 4

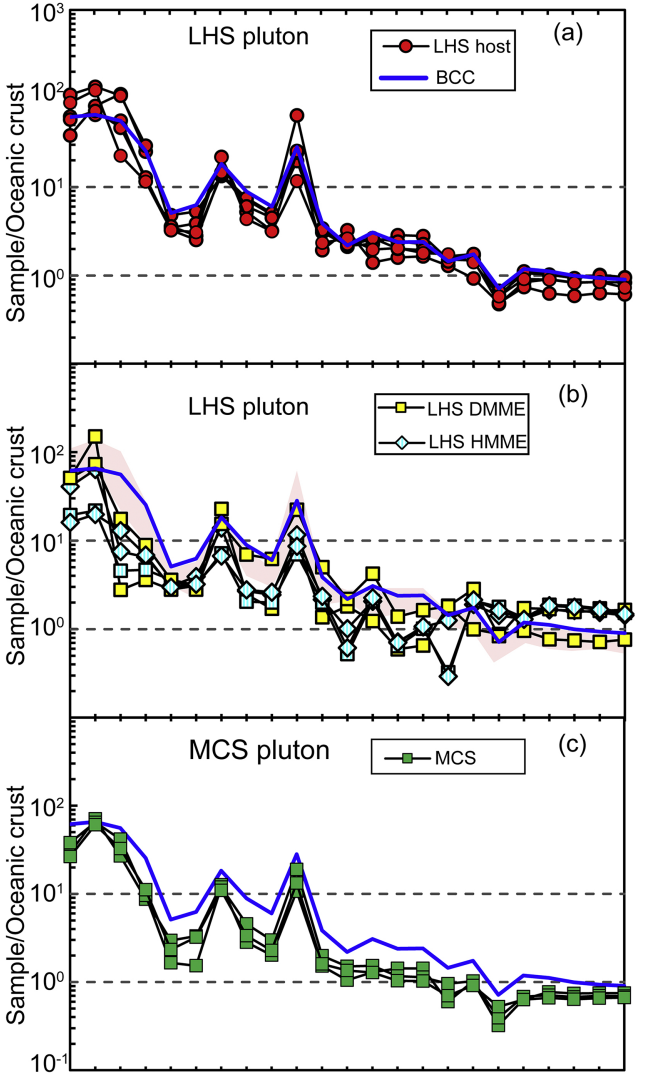
LHS pluton
(a)
LHS host
BCC
LHS pluton
(b)
LHS DMME
LHS HMME
MCS pluton
(c)
MCS
Sample/Oceanic crust
Ba Rb Th U Nb Ta K La Ce Pb Pr Sr Nd Zr Hf P Sm Ti Eu Tb Dy Y Yb

Figure 5

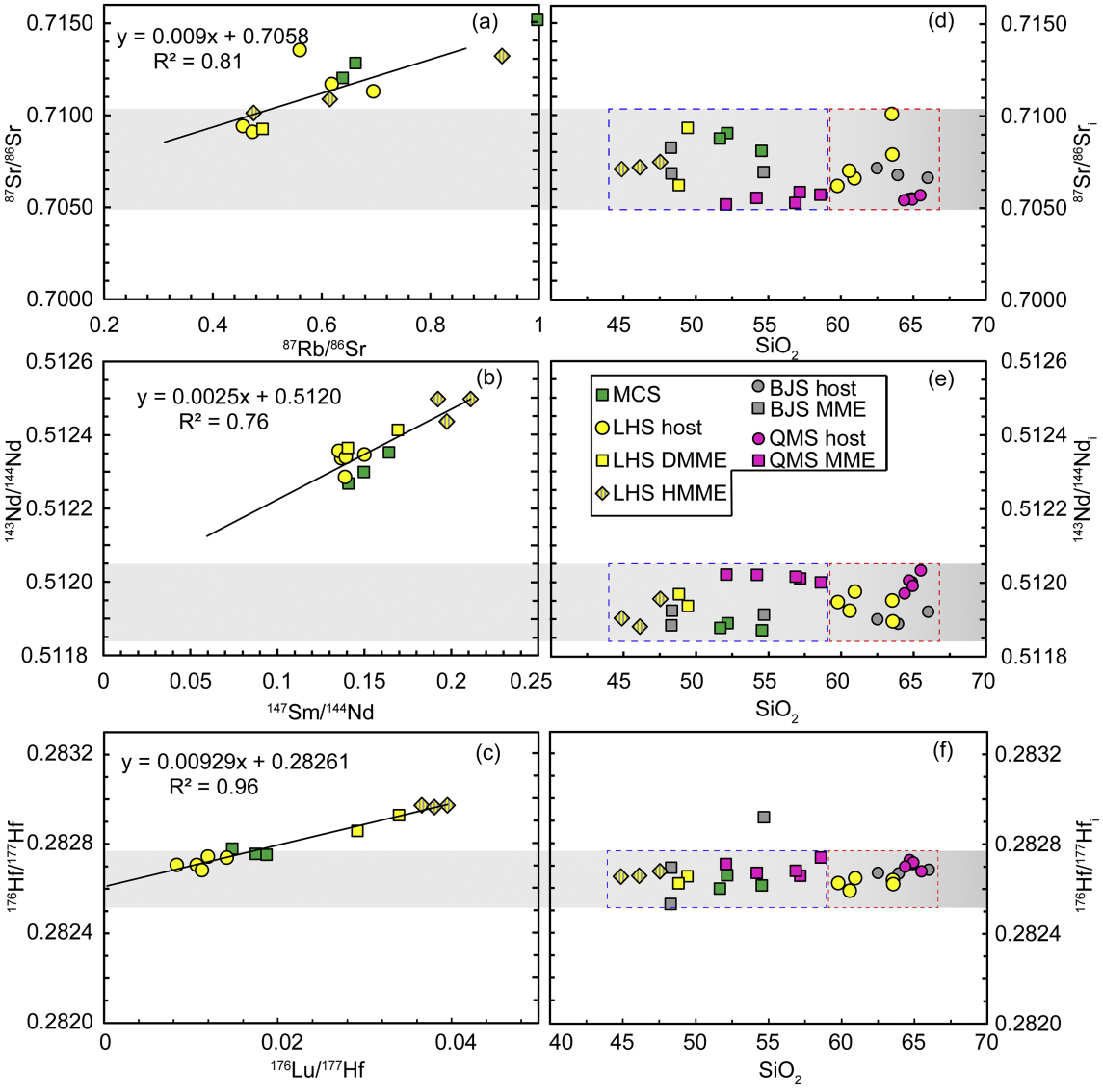
(a)
y = 0.009x + 0.7058
R² = 0.81
$^{87}Sr/^{86}Sr$
$^{87}Rb/^{86}Sr$
(b)
y = 0.0025x + 0.5120
R² = 0.76
$^{143}Nd/^{144}Nd$
$^{147}Sm/^{144}Nd$
(c)
y = 0.00929x + 0.28261
R² = 0.96
$^{176}Hf/^{177}Hf$
$^{176}Lu/^{177}Hf$
(d)
$^{87}Sr/^{86}Sr_i$
SiO_2
(e)
MCS
LHS host
LHS DMME
LHS HMME
BJS host
BJS MME
QMS host
QMS MME
$^{143}Nd/^{144}Nd_i$
SiO_2
(f)
$^{176}Hf/^{177}Hf_i$
SiO_2

Figure 6

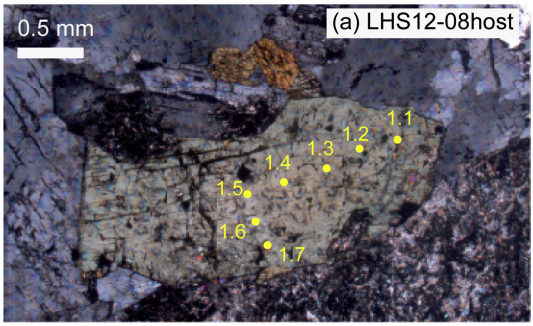
0.5 mm
(a) LHS12-08host
1.1
1.2
1.3
1.4
1.5
1.6
1.7

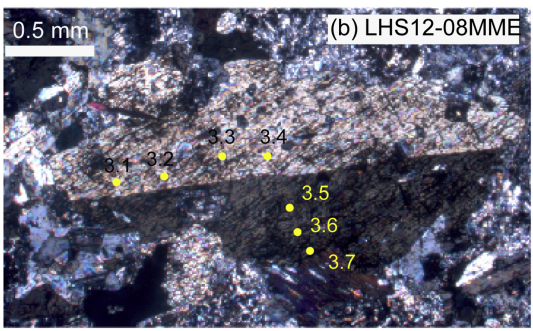
0.5 mm
(b) LHS12-08MME
3.1
3.2
3.3
3.4
3.5
3.6
3.7

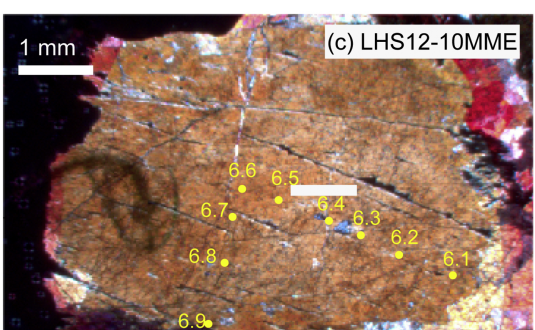
1 mm
(c) LHS12-10MME
6.1
6.2
6.3
6.4
6.5
6.6
6.7
6.8
6.9

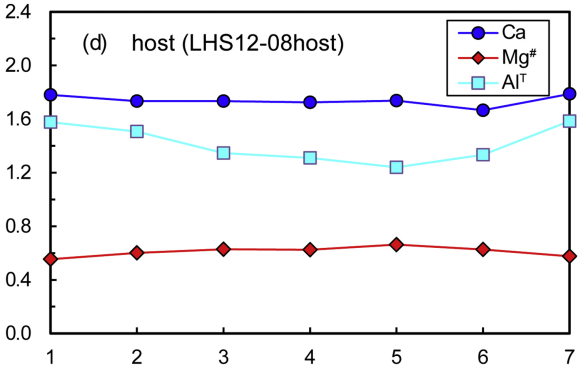
(d) host (LHS12-08host)
Ca
Mg#
AlT
2.4
2.0
1.6
1.2
0.8
0.4
0.0
1
2
3
4
5
6
7

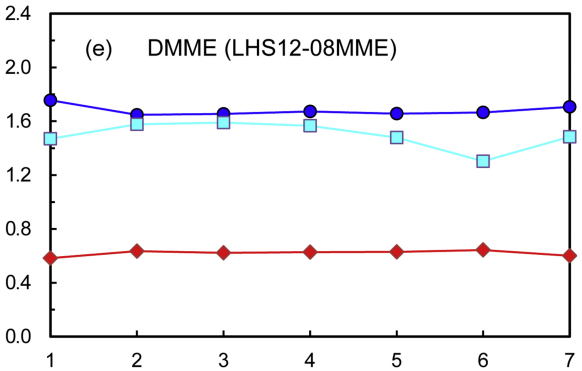
(e) DMME (LHS12-08MME)
2.4
2.0
1.6
1.2
0.8
0.4
0.0
1
2
3
4
5
6
7

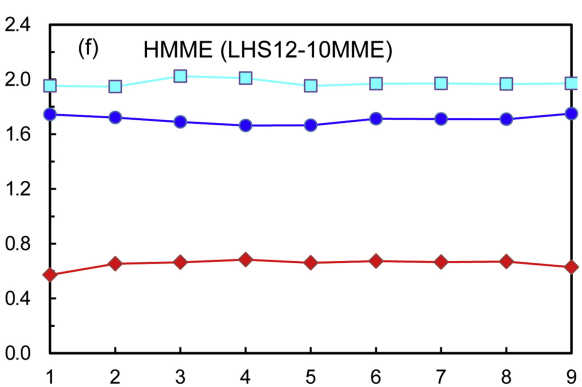
(f) HMME (LHS12-10MME)
2.4
2.0
1.6
1.2
0.8
0.4
0.0
1
2
3
4
5
6
7
8
9

Figure 7

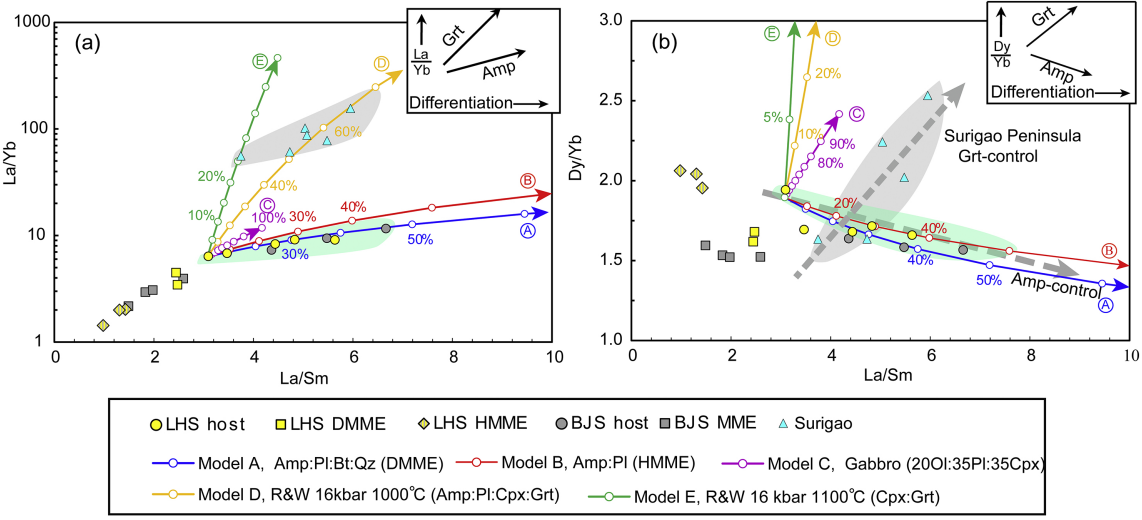
(a)
La/Yb
La/Sm
La
Yb
Grt
Amp
Differentiation
(b)
Dy/Yb
La/Sm
Dy
Yb
Surigao Peninsula
Grt-control
Amp-control
LHS host
LHS DMME
LHS HMME
BJS host
BJS MME
Surigao
Model A, Amp:Pl:Bt:Qz (DMME)
Model B, Amp:Pl (HMME)
Model C, Gabbro (20Ol:35Pl:35Cpx)
Model D, R&W 16kbar 1000℃ (Amp:Pl:Cpx:Grt)
Model E, R&W 16 kbar 1100℃ (Cpx:Grt)

Figure 8

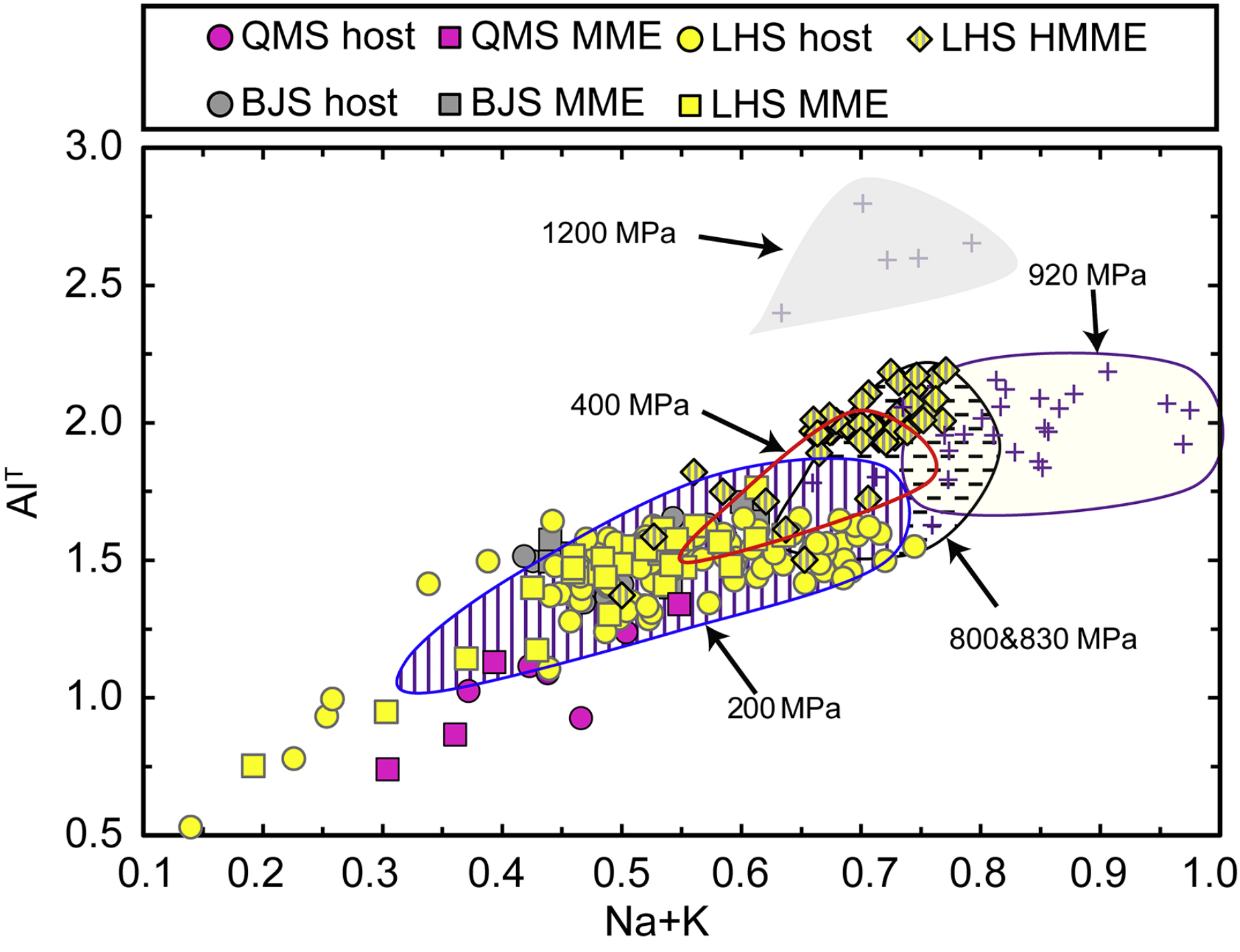
QMS host
QMS MME
LHS host
LHS HMME
BJS host
BJS MME
LHS MME
1200 MPa
920 MPa
400 MPa
800&830 MPa
200 MPa
AlT
Na+K
3.0
2.5
2.0
1.5
1.0
0.5
0.1
0.2
0.3
0.4
0.5
0.6
0.7
0.8
0.9
1.0

Figure 9

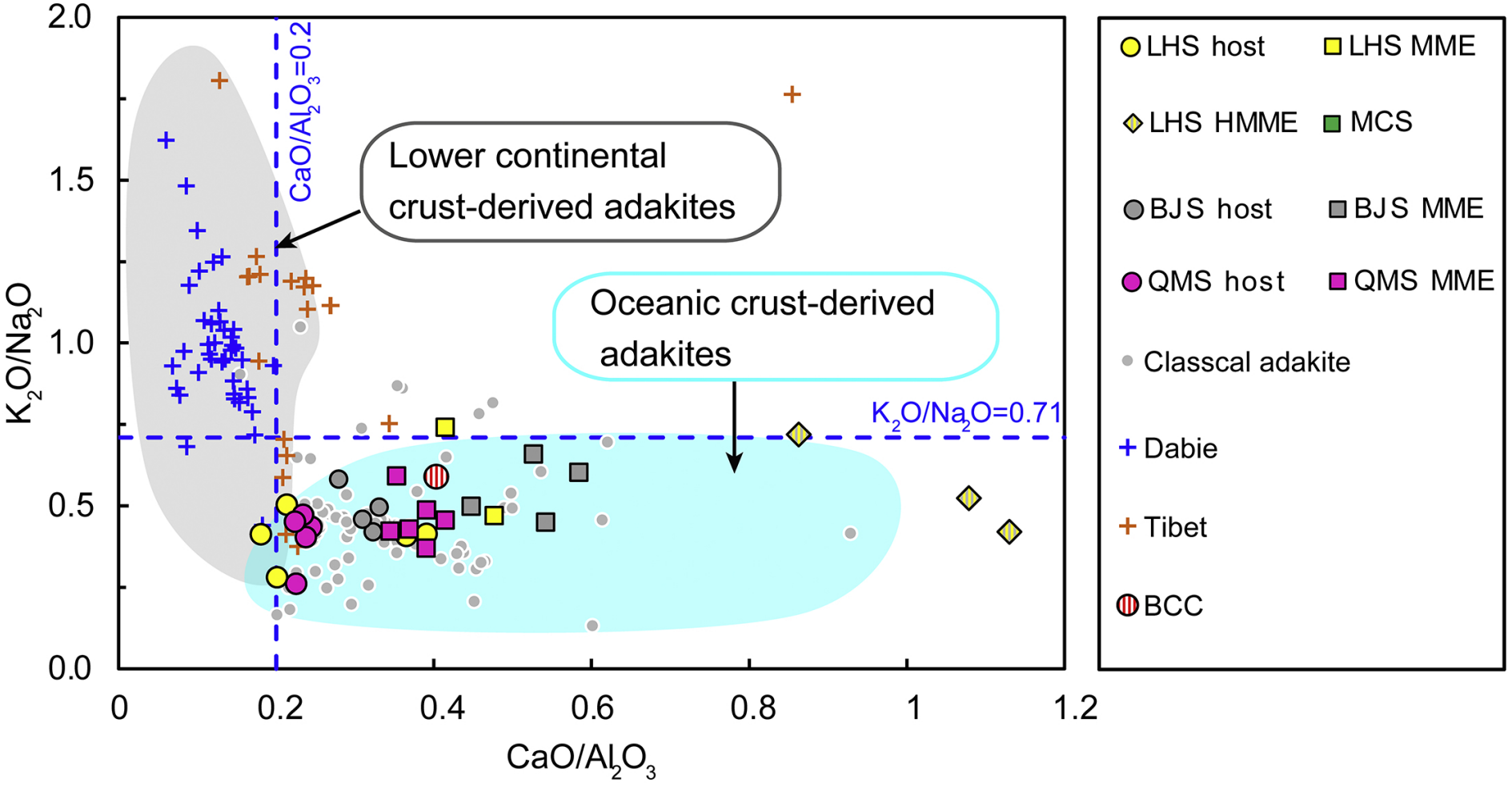
2.0
1.5
1.0
0.5
0.0
0
0.2
0.4
0.6
0.8
1
1.2
K2O/Na2O
CaO/Al2O3
CaO/Al2O3=0.2
K2O/Na2O=0.71
Lower continental crust-derived adakites
Oceanic crust-derived adakites
LHS host
LHS MME
LHS HMME
MCS
BJS host
BJS MME
QMS host
QMS MME
Classcal adakite
Dabie
Tibet
BCC

Figure 10

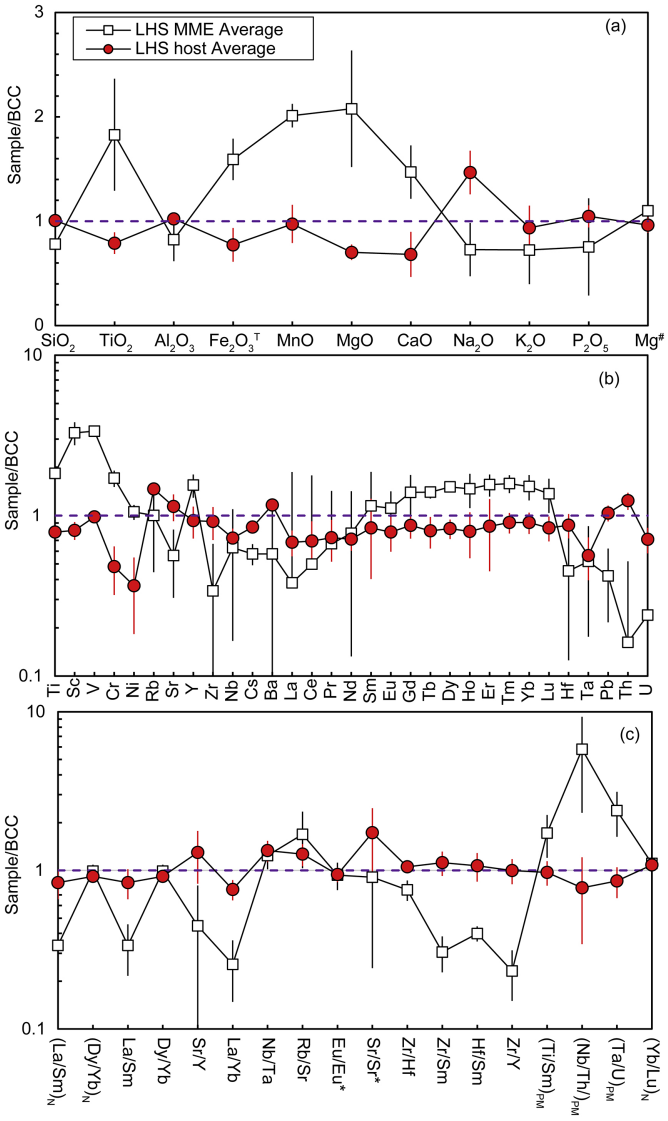
LHS MME Average
LHS host Average
(a)
Sample/BCC
3
2
1
0
SiO2
TiO2
Al2O3
Fe2O3T
MnO
MgO
CaO
Na2O
K2O
P2O5
Mg#
(b)
10
1
0.1
Ti
Sc
V
Cr
Ni
Rb
Sr
Y
Zr
Nb
Cs
Ba
La
Ce
Pr
Nd
Sm
Eu
Gd
Tb
Dy
Ho
Er
Tm
Yb
Lu
Hf
Ta
Pb
Th
U
(c)
(La/Sm)N
(Dy/Yb)N
La/Sm
Dy/Yb
Sr/Y
La/Yb
Nb/Ta
Rb/Sr
Eu/Eu*
Sr/Sr*
Zr/Hf
Zr/Sm
Hf/Sm
Zr/Y
(Ti/Sm)PM
(Nb/Th)PM
(Ta/U)PM
(Yb/Lu)N

Figure 11